HBr Uptake on Ice: Uptake Coefficient, H_2O/HBr Hydrate Formation, and H_2O Desorption Kinetics

P. K. Hudson,[†] K. L. Foster,[†] M. A. Tolbert,[†] and S. M. George*[,‡]

Department of Chemistry and Biochemistry and CIRES, University of Colorado, Boulder, Colorado 80309

S. R. Carlo and V. H. Grassian*

Department of Chemistry, University of Iowa, Iowa City, Iowa 52242

Received: July 27, 2000; In Final Form: November 15, 2000

HBr uptake on thin ice films was examined using laser-induced thermal desorption (LITD), temperature-programmed desorption (TPD) and Fourier transform infrared (FTIR) spectroscopy techniques. LITD was used to determine the uptake coefficient in situ during low HBr exposures as a function of HBr pressure and ice film temperature. The HBr uptake coefficient on ice was $\gamma = 0.61 \pm 0.06$ at 140 K and $\gamma = 0.24 \pm 0.05$ at 100 K at low HBr coverages for HBr pressures ranging from 3×10^{-8} to 1.4×10^{-7} Torr. TPD and FTIR were used to examine HBr uptake on ice at higher HBr exposures. TPD studies observed that thin ice films exposed to HBr at 140 K saturated with HBr after large exposures and formed an HBr hydrate with an H_2O:HBr ratio of ~3.6:1. FTIR measurements monitored the development of the H_3O^+ bending vibration versus HBr exposure on ice. Saturation of the integrated absorbance for this H_3O^+ bending vibration was observed after large HBr exposures. The uptake of HBr on ice also had a profound effect on H_2O desorption from ice. H_2O desorbed at higher temperatures in the presence of HBr. The zero-order kinetics for H_2O desorption from pure ice were $E_d = 13.4$ kcal mol^{-1} and $\nu_0 = 1.9 \times 10^{32}$ cm^{-2} s^{-1}. The zero-order kinetics for H_2O desorption from the HBr hydrate formed after saturation HBr exposures were $E_d = 10.6$ kcal mol^{-1} and $\nu_0 = 6.3 \times 10^{27}$ cm^{-2} s^{-1}.

I. Introduction

Rapid and complete ozone destruction is observed in the springtime Arctic boundary layer.[1−3] The measured anticorrelation between filterable bromide and ozone suggests that catalytic gas-phase bromine reactions are responsible for the dramatic ozone loss.[1] In support of this suggestion, high levels of BrO[4,5] and photolyzable bromine[6] are also observed during ozone depletion events. The proposed source of these active bromine species is sea salt.[7−10] In one mechanism, HOBr reacts catalytically with sea salt particles to produce active forms of bromine such as Br_2 and BrCl.[9] Another possible mechanism for active bromine production is a dark reaction of ozone with bromide in sea salt ice.[10] Upon photolysis of Br_2 and BrCl, bromine radicals form and can catalytically destroy ozone.

One problem with the above mechanisms is that active bromine can also rapidly transform into the HBr reservoir species.[7,11] For example, HBr can be formed by reaction of Br with formaldehyde, CH_2O, or hydroperoxide radical, HO_2:[12]

$$Br + CH_2O \rightarrow HBr + CHO \quad (1)$$

$$Br + HO_2 \rightarrow HBr + O_2 \quad (2)$$

Recent measurements in the springtime Arctic boundary layer show large amounts of formaldehyde.[13] Assuming 400 ppt of CH_2O, the lifetime of Br defined by reaction 1 is ~2 min. Consequently, reaction 1 can severely limit the ability of Br to destroy ozone.

Active bromine must be recycled from the HBr reservoir species to maintain catalytic ozone destruction.[11] One possible process involves heterogeneous reactions to release photochemically labile bromine species. Probable reactions for the recycling include:[14−16]

$$HBr + HOCl \rightarrow BrCl + H_2O \quad (3)$$

$$HBr + HOBr \rightarrow Br_2 + H_2O \quad (4)$$

Possible surfaces for reactions 3 and 4 in the troposphere include sulfuric acid aerosols, ice particles and snowpack. These reactions have been examined on ice under stratospheric conditions and have proven to be effective in releasing BrCl and Br_2.[14−16] A full understanding of these reactions requires information on the interaction of HBr with ice surfaces.

In this work, the uptake of HBr with ice surfaces was measured from 90 to 140 K. Previous studies have examined HBr uptake on ice surfaces at higher temperatures of 180−233 K.[17−21] These studies all relied on gas-phase measurements to infer HBr uptake. In contrast, we have performed laboratory studies of the HBr interaction with ice using techniques that probe the condensed phase. Laser-induced thermal desorption (LITD) was utilized to measure the HBr uptake coefficient on ice as a function of ice temperature and HBr pressure. Temperature-programmed desorption (TPD) was used to determine the H_2O/HBr composition and to examine the effect of HBr on the H_2O desorption kinetics from ice. Fourier transform infrared (FTIR) spectroscopy was employed to monitor the saturation of the ice films with HBr. These studies complement

[†] CIRES.
[‡] Department of Chemistry and Biochemistry.

10.1021/jp002700w CCC: $20.00
Published on Web 01/06/2001

recent TPD and FTIR studies of H_2O/HBr thin films of varying stoichiometry[22] and FTIR investigations of HBr uptake on ice.[23]

II. Experimental Section

A. Vacuum Chamber and HBr Exposures. Experiments at the University of Colorado were conducted in an ultrahigh vacuum chamber equipped with a UTI-100C mass spectrometer, an ionization gauge, and an absolute pressure capacitance manometer (MKS Baratron Type 690A.1 TRB).[24,25] The capacitance manometer measures absolute pressures above 1×10^{-6} Torr. An Al_2O_3 (0001) substrate was attached to the bottom of a liquid nitrogen cooled cryostat and suspended in the middle of the chamber.[26] The 12×20 mm Al_2O_3 crystal was 0.5 mm thick with a 5° wedge between the front and back faces for facile optical interference measurements.[27] The back face was coated with 3000 Å of molybdenum for resistive heating of the substrate.[26]

Ice films were deposited by backfilling H_2O vapor onto the cooled Al_2O_3 substrate at 140 K. The H_2O vapor source was an HPLC grade reservoir of liquid H_2O (Fisher Scientific) purified by a series of liquid nitrogen freeze−pump−thaw cycles. HBr gas (Matheson, 99.95%) was transported through a gas line to a glass coldfinger in liquid nitrogen for purification. The principal impurities of the HBr sample are H_2 and Br_2. H_2 does not condense at liquid nitrogen temperatures and was removed by pumping the vapor above the condensed HBr sample. Crystalline Br_2 has a low vapor pressure relative to HBr. Br_2 remained condensed when the liquid nitrogen was removed and the coldfinger was allowed to warm to fill the glass gas line with HBr gas.

The purity of the condensed H_2O and HBr multilayers was determined by mass spectrometry. The films were analyzed by LITD at masses $m/e = 1-100$ to check for possible impurities. For the HBr multilayers, mass signals $m/e = 79-82$ were assigned to the isotopes of HBr at 80 and 82 amu and Br fragments at 79 and 81 amu. H_2O impurities in the HBr multilayer were present at levels of <10%. All impurities in the ice films were negligible.

Ion gauge measurements were recorded before and after backfilling HBr into the chamber to determine the experimental HBr pressures. The absolute pressure capacitance manometer was utilized to calibrate the ion gauge measurements. This calibration was performed by recording ion gauge and Baratron readings for HBr pressures between 1×10^{-8} and 1×10^{-4} Torr. The HBr pressure was used to define the HBr exposures in Langmuir (L) where $1\ \text{L} = 1 \times 10^{-6}$ Torr s.

Experiments performed at the University of Iowa were carried out in an ultrahigh-vacuum (UHV) chamber with a base pressure of 5×10^{-10} Torr.[28] This UHV chamber was equipped with an ionization gauge, a cylindrical mirror analyzer for Auger electron spectroscopy, a quadrupole mass spectrometer for TPD and residual gas analysis, an ion sputtering gun for sample cleaning and three variable leak valves for introducing gases into the chamber. An Ag(110) substrate was mounted in the UHV chamber on a tantalum cup. This tantalum cup was attached to a liquid nitrogen cooled Cu block that allowed cooling to ~95 K. The temperature of the Ag(110) substrate during the experiments was measured by a chromel−alumel thermocouple.

B. Temperature-Programmed Desorption and Laser-Induced Thermal Desorption. Temperature-programmed desorption (TPD) experiments at the University of Colorado (Figures 6−8) were used to monitor HBr uptake on the ice films. TPD spectra were recorded after ice films at 90−140 K were exposed to HBr at pressures between 3×10^{-8} and 7×10^{-7} Torr for times between 15 s and 45 min. After HBr exposure, the chamber was evacuated and the sample was cooled to 85 K before recording the TPD spectrum.

The UTI-100C quadrupole mass spectrometer was used to monitor the evolution of desorbed species from the Al_2O_3 substrate. Desorption measurements were performed with the Al_2O_3 crystal facing the ionizer of the mass spectrometer. A constant heating rate of 1.0 K/s was used for the TPD spectra performed at the University of Colorado. The temperature was measured with a chromel−alumel thermocouple attached to the front of the Al_2O_3 crystal using ceramic glue from Aremco.

For temperature-programmed desorption (TPD) experiments at the University of Iowa (Figure 3), the Ag(110) substrate was resistively heated at a rate of 1.5 K/s. A UTI-100C quadrupole mass spectrometer recorded the TPD spectra. The stoichiometry of the H_2O/HBr films was calculated using the H_2O and HBr TPD peak areas for $m/e = 18$ and 82, respectively. The TPD peak areas were calibrated using two correction factors. The first correction factor accounted for the sensitivity of the ionization gauge for each gas. These sensitivity factors were determined earlier in experiments using an absolute capacitance manometer at the University of Colorado.

The second correction factor was the relative mass spectrometer response to each gas. This correction factor was determined by backfilling the chamber with known pressures of each gas measured using the ionization gauge and recording the mass spectrum. The peak height was then calibrated versus gas pressure. These two calibration factors allowed the H_2O:HBr ratio to be calculated from the integrated area under the respective TPD curves.

Laser-induced thermal desorption (LITD) techniques were used to measure the HBr uptake coefficient on ice films at the University of Colorado. A pulsed Lumonics CO_2 TEA laser operating at $\lambda = 10.6\ \mu$m was modified for TEM-00 operation.[29] The CO_2 laser pulse had a Gaussian distribution and a pulse width of 100 ns. The CO_2 laser beam was attenuated to 55 mJ and expanded to a 2 cm diameter with a ZnSe beam expander. The beam was then focused using a ZnSe lens with a 104 cm focal length.

The CO_2 laser beam entered the chamber through a ZnSe window and intersected the surface at 45° from the surface normal. The CO_2 laser energy was absorbed by the H_2O multilayer and the Al_2O_3 substrate[25] and produced a desorption area with a diameter of ~1 mm measured using the spatial autocorrelation method.[30] To maximize surface sensitivity, the mass spectrometer and substrate were positioned for line-of-sight detection of the desorbed surface species. The LITD signals from H_2O and HBr multilayer films were calibrated using optical interference measurements. These calibrations were then used to convert the measured HBr and H_2O LITD signals into coverages.

C. Coverage Calibration Using Optical Interference. The TPD and LITD signals at the University of Colorado were calibrated by optical interference studies of multilayer films.[27,31,32] Briefly, the specular reflection of a helium neon (HeNe) laser that intersected the Al_2O_3 substrate at a near normal angle of incidence was measured during film growth. The intensity of the reflected beam plotted versus film growth results in a sinusoidal interference pattern. The film thickness, x, is obtained using:

$$x = m\lambda/2n(T) \tag{5}$$

where m is the number of periods of oscillation, $\lambda = 6328$ Å is the wavelength of the HeNe laser, and $n(T)$ is the temperature-

dependent real refractive index.[32] Using this technique, one-half of an oscillation period during H_2O multilayer deposition at 140 K represents a film thickness of 1244 Å. One-half of an oscillation period during HBr multilayer deposition at 82 K represents a film thickness of 1058 Å.

The integrated areas of the H_2O and HBr TPD peaks and LITD signals were plotted versus film thickness determined using the optical interference technique. The correlation between film thicknesses and TPD peak areas or LITD signals was linear. This calibration was used to quantify the H_2O and HBr coverages obtained from TPD and LITD experiments. The H_2O coverage was determined from the measured H_2O multilayer thickness using a density of $\rho = 0.93$ g/cm^3 and a refractive index of $n = 1.31$ at $T \geq 140$ K.[32] The correlation between the HBr LITD signals and the HBr film thicknesses was linear over the entire thickness range from 280 to 1120 Å. On the basis of the statistics of the linear fit, the uncertainty of the HBr coverages obtained from the HBr LITD signals was ±10%.

The HBr multilayer was formed by depositing HBr on the Al_2O_3 substrate at 82 K. Calibration of the HBr mass signal at $m/e = 80$ is difficult because there are no literature values for the real refractive index and density of condensed HBr multilayers at 82 K. Consequently, the refractive index of the HBr multilayers was determined by monitoring the maxima and minima in the HeNe reflectance from the HBr multilayer on the Al_2O_3 substrate during HBr deposition. This method has been used earlier to determine the refractive indices of ice[32] and nitric acid hydrates.[31] The refractive index of HBr multilayers determined by these optical interference experiments was $n = 1.46$.

The measured refractive index of $n = 1.46$ was used to determine the density of the HBr multilayers deposited at 82 K using the Lorentz−Lorenz relationship.[33] The molar refractivity of HBr was determined from the refractive index of HBr/H_2O solutions assuming that the molar refractivities of the components are additive.[33] The molar refractivity of a two-component H_2O and HBr film is given by Lorentz−Lorenz analysis as[33]

$$A_{\text{film}} = \chi_{H_2O}A_{H_2O} + \chi_{HBr}A_{HBr} = [w_a(n^2 - 1)]/[\rho_a(n^2 + 2)] \quad (6)$$

In this equation, χ is the mole fraction of H_2O or HBr and ρ_a is the density of the film. The average molecular weight of the film, w_a, is calculated by $w_a = \chi_{H_2O}m_{H_2O} + \chi_{HBr}m_{HBr}$ where m is the molecular mass.

A molar refractivity of $A_{H_2O} = 3.72$ cm^3/mol was determined by extrapolating the calculated A_{film} values to 0 wt %. This value is in good agreement with other literature values.[33,34] An HBr molar refractivity of $A_{HBr} = 12.1$ cm^3/mol was then determined by fitting eq 6 to the known densities and refractive indices for HBr/H_2O solutions.[35] A_{HBr} was also determined by extrapolating the densities and refractive indices of the HBr/H_2O solutions to 100 wt % HBr. These calculations yielded a molar refractivity of $A_{HBr} = 11.6$ cm^3/mol. The average of the two calculated molar refractivities, $A_{HBr} = 11.9$ cm^3/mol was subsequently used to determine the HBr density. The HBr density was calculated to be $\rho = 1.9$ g/cm^3 using the measured refractive index of $n = 1.46$ for the HBr multilayer at 82 K. This density was used for the calibration of the HBr LITD signals.

Another employment of the Lorentz−Lorenz analysis uses individual molar refractivities of the H and Br atomic components. The molar refractivity for a single constituent is defined as[33]

$$A_{HBr} = A_H + A_{Br} = [w(n^2 - 1)]/[\rho(n^2 + 2)] \quad (7)$$

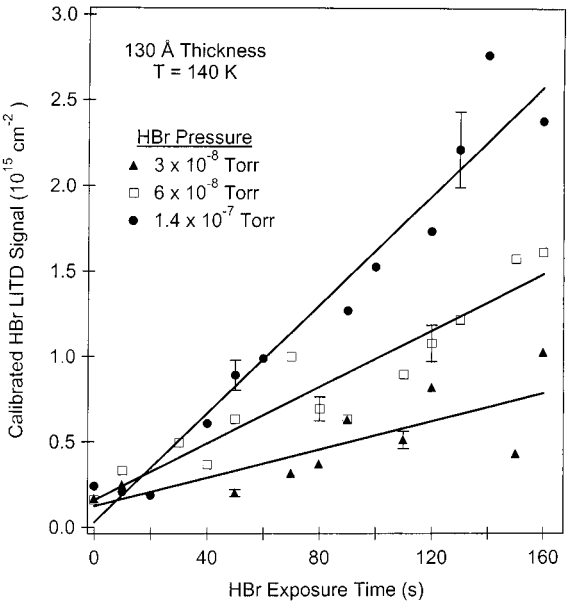

Figure 1. Calibrated HBr laser-induced thermal desorption signals versus HBr exposure time at HBr pressures of 3×10^{-8}, 6×10^{-8} and 1.4×10^{-7} Torr from a 130 Å thick ice film at 140 K. The solid lines show the linear least-squares fits to the data.

In this expression, w is the molecular weight and ρ is the HBr density. Using $w = 81$ g/mol and $n = 1.46$, a density of $\rho = 2.27$ g/cm^3 is calculated using atomic molar refractivities of $A_H = 1.028$ cm^3/mol and $A_{Br} = 8.741$ cm^3/mol.[36] This density would increase the measured HBr uptake coefficients by ~20%.

D. Reflectance Absorption Infrared Spectroscopy. A Mattson 6021 Galaxy FTIR spectrometer equipped with external beam capabilities and a narrowband mercury-cadmium-telluride (MCT) detector was used for reflectance infrared measurements at the University of Iowa.[28] The lower limit of the spectral range was limited to ~750 cm^{-1} by the MCT detector. Each absorbance spectrum was acquired by summing 1000 sample scans at an instrument resolution of 4 cm^{-1}. The reference was the spectrum of the clean Ag(110) substrate acquired under the same conditions.

III. Results

A. HBr Uptake Coefficient on Ice. The initial HBr adsorption kinetics were measured in real time using LITD techniques at the University of Colorado. Figure 1 shows the calibrated HBr LITD signals for HBr uptake on an ice film at 140 K for HBr pressures of 3×10^{-8}, 6×10^{-8} and 1.4×10^{-7} Torr. The error bars on selected points represent the calibration uncertainty of ±10%. The ice film was initially deposited on the Al_2O_3 substrate at 140 K. These results are consistent with HBr uptake that is first-order with respect to HBr pressure. The maximum HBr exposure at 1.4×10^{-7} Torr for 160 s is 22.4 L. This exposure yields an HBr coverage of ~2.5×10^{15} cm^{-2}.

The HBr uptake coefficient, γ, is defined as the number of HBr molecules that adsorb onto the ice film divided by the total exposure of HBr molecules on the ice film. The HBr flux, $\Phi = (1/4)\rho\upsilon$, was determined using results from kinetic gas theory at 298 K where $\rho = n/V = P/RT$ and $\upsilon = (8RT/\pi m)^{1/2}$. The HBr exposure is equal to the flux multiplied by the exposure time. The linear fits to the HBr coverages versus exposure time for the three HBr adsorption experiments shown in Figure 1 yield an average HBr uptake coefficient of $\gamma = 0.61 \pm 0.06$ at 140 K. The linear fits do not go through the origin at zero HBr

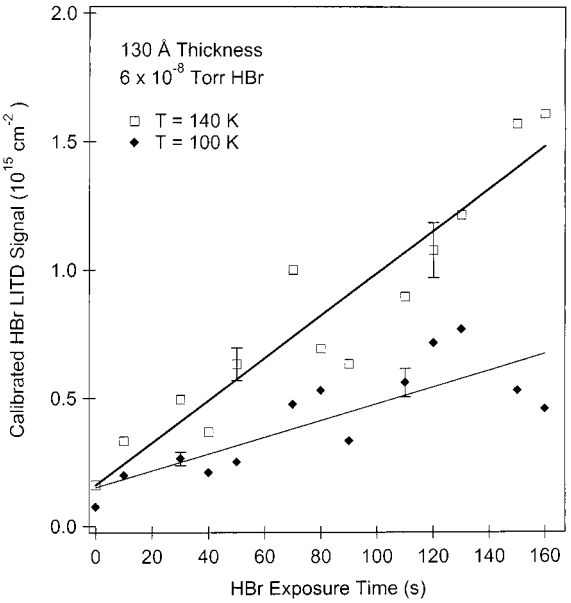

Figure 2. Calibrated HBr laser-induced thermal desorption signals versus HBr exposure time at an HBr pressure of 6×10^{-8} Torr from a 130 Å thick ice film at 100 and 140 K. The solid lines show the linear least-squares fits to the data.

exposure presumably because of small HBr background pressures in the vacuum chamber.

The uptake of HBr by the ice films was also observed to be dependent on ice film temperature. Figure 2 displays the calibrated HBr LITD signals for HBr uptake on ice at an HBr pressure of 6×10^{-8} Torr at 100 and 140 K. The ice films for both of these experiments were deposited on the Al_2O_3 substrate at 140 K. The HBr uptake is slower at 100 K than 140 K. The HBr uptake coefficient decreases to $\gamma = 0.24 \pm 0.05$ for the measurement at 100 K. The linear fits again do not go through the origin at zero HBr exposure because of finite HBr background pressures.

B. H_2O and HBr Desorption versus HBr Exposure. Ice films with a thickness of 140 Å were deposited on Ag(110) at 140 K. These ice films were then exposed to HBr at 140 K. Figure 3 shows the H_2O TPD signal at $m/e = 18$ and the HBr TPD signal at $m/e = 82$ versus HBr exposure using HBr pressures ranging from 1×10^{-7} Torr to 5×10^{-7} Torr. The pure ice displays an H_2O desorption peak at 168 K. Upon exposure to HBr, Figure 3a reveals that the H_2O TPD peak moves to slightly lower temperatures of 164−167 K. A second higher temperature H_2O peak also appears at 174−178 K and grows versus HBr exposure.

The HBr TPD spectra in Figure 3b display a peak between 174 and 178 K. The HBr peak grows and shifts to slightly higher temperature versus HBr exposure. The HBr TPD peaks coincide with the higher temperature H_2O TPD peaks. The correlation of these H_2O and HBr TPD peaks suggests that these desorption species evolve from the same H_2O/HBr hydrate.

C. FTIR Spectra versus HBr Exposure. To analyze the effect of HBr on the ice films using FTIR spectroscopy, ice films with a thickness of 345 Å were deposited on Ag(110) at 140 K. HBr was then exposed to the ice film at 140 K. Figure 4 shows the changes in the FTIR spectra versus HBr exposure using HBr pressures varying from 1×10^{-7} Torr to 1×10^{-6} Torr. After low HBr exposures, the H_2O bending mode (ν_2) at 1641 cm^{-1} decreased in intensity and another absorption feature progressively appeared near 1747 cm^{-1}. This absorption feature has been previously assigned to the H_3O^+ bending mode .[37,38]

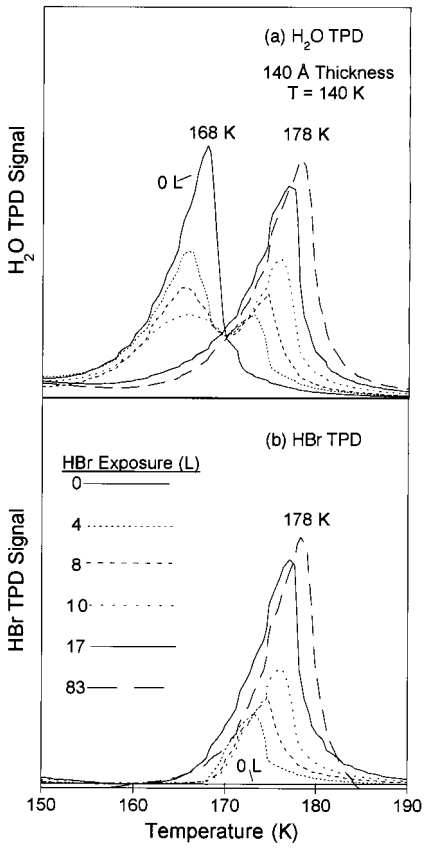

Figure 3. Temperature-programmed desorption signals for (a) H_2O ($m/e = 18$) and (b) HBr ($m/e = 82$) from a 140 Å thick ice film versus HBr exposure at 140 K. The heating rate was 1.5 K/s.

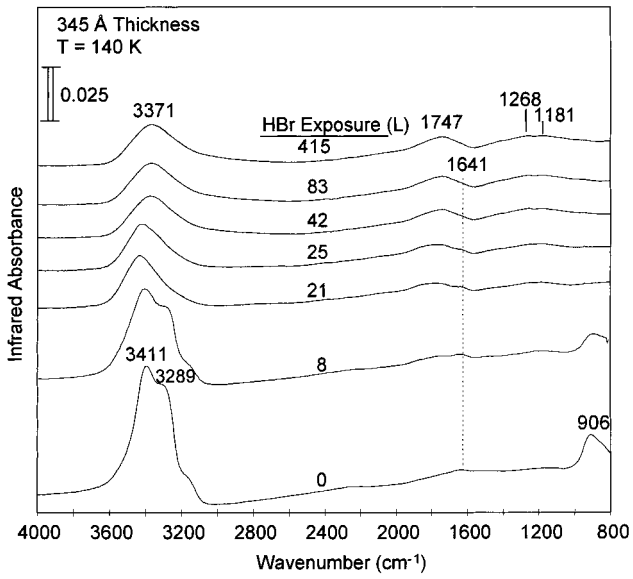

Figure 4. Reflection−absorption infrared spectra of a 345 Å thick ice film versus HBr exposure at 140 K.

Figure 4 shows that the H_2O libration (ν_7) was observed at 906 cm^{-1}. This feature disappears very quickly versus HBr exposure. Very pronounced changes are also observed in the O−H stretching region. Initially a single sharp band is observed at 3411 cm^{-1} with a shoulder at 3289 cm^{-1}. These spectral features are consistent with a polycrystalline ice sample.[39,40] After exposure to HBr, these O−H stretching features decrease in intensity and form a single peak. This new peak initially shifts to slightly higher energy and then shifts to lower energy with a peak at 3371 cm^{-1} after HBr saturation. The broadness of

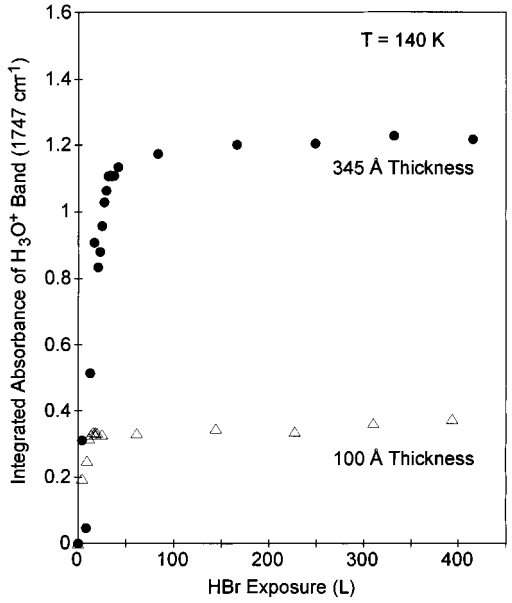

Figure 5. Integrated absorbance of H_3O^+ band at 1747 cm^{-1} versus HBr exposure at 140 K for ice film thicknesses of 100 and 345 Å.

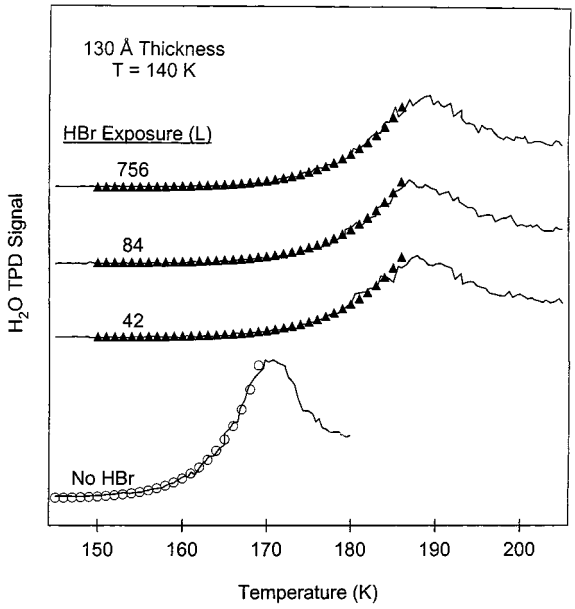

Figure 6. H_2O temperature-programmed desorption signal from a 130 Å thick ice film versus HBr exposure at 140 K. The heating rate was 1.0 K/s. The open circles and solid triangles display the predicted desorption rates from the desorption kinetic parameters.

this vibrational band suggests the formation of an amorphous H_2O/HBr film.[39]

HBr uptake was monitored using the integrated absorbance of the H_3O^+ bending mode at 1747 cm^{-1}. Figure 5 shows the integrated absorbance versus HBr exposure at 140 K for ice film thicknesses of 100 and 345 Å. The estimated uncertainty for the integrated absorbance is only ±0.02. Comparison of these data indicate that the ice film with a thickness of 345 Å has a final integrated intensity ~3.5 times larger than the integrated intensity of the 100 Å film. This behavior indicates that HBr uptake at 140 K is proportional to ice film thickness. In addition, the finite saturation levels imply that an H_2O/HBr hydrate has been formed with a definite stoichiometry.

D. H_2O Desorption from Ice Films Exposed to HBr. H_2O desorption from ice films exposed to HBr was different than H_2O desorption from pure ice films. Figure 6 shows an H_2O TPD spectrum from a pure ice film with a thickness of 130 Å that was deposited at 140 K. A single H_2O TPD peak at ~170 K was observed for this pure ice film. These results are consistent with numerous earlier studies of H_2O desorption from ice multilayers.[38] The open circles show the fit of zero-order kinetics to the H_2O desorption data.

Figure 6 also displays the effect of HBr on the H_2O TPD spectrum after the ice films were exposed to HBr exposures of 42, 84, and 756 L. The H_2O desorption is shifted to higher temperatures after these HBr exposures and the low-temperature TPD peak at 170 K for H_2O desorption from pure ice is lost. All the H_2O desorbs from the higher temperature H_2O peak at ~190 K. The solid triangles show the fit of zero-order kinetics to the H_2O desorption data after the HBr exposures.

H_2O desorption was also examined after a constant HBr exposure on various ice film thicknesses. Figure 7 shows H_2O TPD signals after an HBr exposure of 32 L at 140 K. For an ice film thickness of 105 Å, only the high-temperature H_2O TPD peak is observed at ~190 K. As the ice film thickness increases, a lower temperature H_2O TPD peak at 175−180 K progressively emerges and dominates the H_2O TPD spectrum at the largest ice film thickness of 670 Å.

Additional H_2O TPD experiments were performed to determine whether H_2O desorption was dependent on the initial location of HBr in the ice film. An ~130 Å thick ice film was

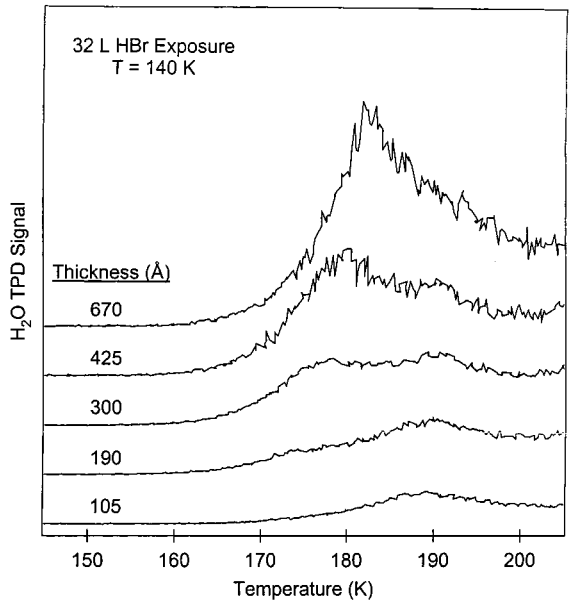

Figure 7. H_2O temperature-programmed desorption signals after a 32 L HBr exposure on ice films of various thickness at 140 K. The heating rate was 1.0 K/s.

exposed to 24 L HBr at 140 K. After HBr exposure, a second layer of ice with a thickness of ~390 Å was deposited on top of the HBr-exposed ice film. H_2O desorption from this sandwich film was identical to H_2O desorption from an ice film prepared by a 24 L HBr exposure on an ice film thickness of ~520 Å. These results demonstrate that HBr affects the H_2O desorption kinetics both when HBr is deposited on top of an ice film or when HBr is sandwiched inside an ice film.

The effect of temperature on HBr uptake was also explored by H_2O TPD experiments. Figure 8 shows H_2O TPD spectra for ice films with a thickness of 130 Å after exposure to 32 L HBr at various ice film temperatures. All of these ice films were originally deposited on the Al_2O_3 substrate at 140 K. Only a high-temperature H_2O TPD peak at ~190 K is observed after HBr exposure at 140 K. As the ice film temperature decreases,

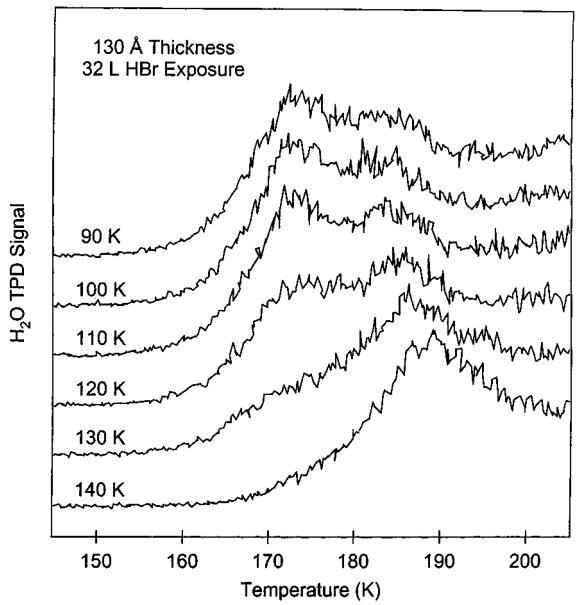

Figure 8. H_2O temperature-programmed desorption signal after a 32 L HBr exposure on a 130 Å ice film at various ice film temperatures.

more H_2O is observed to desorb from the lower temperature H_2O TPD peak at ~175 K.

IV. Discussion

A. HBr Uptake Coefficient. The LITD results shown in Figures 1 and 2 yield an HBr uptake coefficient of $\gamma = 0.61 \pm 0.06$ at an ice film temperature of 140 K and HBr pressures of $\sim 10^{-8}$ Torr. Figure 2 shows that the HBr uptake coefficient decreases to $\gamma = 0.24 \pm 0.05$ at an ice film temperature of 100 K. These results can be compared with previously reported HBr sticking coefficients and uptake coefficients. An initial HBr sticking coefficient of $S = 1.0 \pm 0.05$ was reported by earlier molecular beam measurements conducted at 80−130 K using the King and Wells method.[41] Earlier flow reactor studies observed an initial HBr uptake coefficient on ice with a lower limit of $\gamma > 0.3$ at 200 K.[17] Recent low-pressure flow tube experiments measured an uptake coefficient of $\gamma = 0.03 \pm 0.005$ at $T > 212$ K and $\gamma \geq 0.1$ at $T < 212$ K.[20] A low-pressure Knudsen cell experiment determined uptake coefficients that varied from $\gamma = 0.20-0.34$ at ice film temperatures from 210 to 190 K, respectively.[21] Other Knudsen cell experiments measured an uptake coefficient with a lower limit of $\gamma > 0.02$ at 180−210 K.[23]

HBr uptake on ice can also be compared with HCl uptake on ice. The pure ice surface is known to adsorb HCl with a near unity sticking coefficient. The molecular beam experiments[41−43] and theoretical calculations[44,45] for HCl are all consistent with a near unity sticking coefficient on the pure ice surface for thermal energy HCl beams. Although similar calculations have not yet been conducted for HBr, there should be similar behavior for HCl and HBr. The molecular beam experiments that measured both HCl and HBr obtained an initial sticking coefficient of $S = 1.00 \pm 0.05$ for HBr and an initial sticking coefficient of $S = 0.95 \pm 0.05$ for HCl.[41]

The HBr uptake coefficient determined by the LITD measurements is somewhat less than unity. However, Figures 1 and 2 indicate that the HBr uptake coefficient was measured at HBr coverages ranging from 2.5×10^{14} cm^{-2} to 4×10^{15} cm^{-2}. The number of H_2O molecules in the top bilayer of the basal plane of hexagonal ice is $\sim 1 \times 10^{15}$ cm^{-2}.[46] This coverage can be used to define one monolayer (1 ML). The LITD measurements were performed at HBr coverages from ~0.25 to 4 ML. In contrast, one of the molecular beam measurements of the HCl sticking coefficient was conducted at much lower HCl coverages of ~0.005 ML.[43] The ~0.25 to 4 ML HBr coverages on the ice film during our uptake coefficient measurements may act to lower the uptake coefficient from unity. In support of this explanation, the molecular beam investigations noticed that the HCl sticking coefficient decreased to $S = 0.88 \pm 0.03$ on a HCl-covered ice surface and concluded that HCl blocks the surface sites that are need to adsorb additional HCl molecules.[43]

The reduction of the uptake coefficient to $\gamma = 0.24 \pm 0.05$ at an ice film temperature of 100 K can be interpreted using a similar explanation. The HBr uptake coefficient is dependent on the HBr surface coverage. If HBr can diffuse into the ice bulk, HBr will not block the surface sites responsible for HBr adsorption. HBr would be expected to diffuse into the ice bulk more rapidly at 140 K than 100 K. The steady-state HBr surface coverage during the competing HBr adsorption and HBr diffusion would then be higher at 100 K than at 140 K. Consequently, the HBr uptake coefficient would be expected to be less at 100 K than at 140 K.

Although there are no known measurements of HBr diffusion in ice, there are several measurements for HCl diffusion in ice. Using microtome measurements on macroscopic single-crystal ice samples, HCl diffusion coefficients of $D \sim 5 \times 10^{-12}$ cm^2/s were measured at 235−265 K.[47] Unfortunately, the measured diffusion coefficients were scattered and an Arrhenius analysis was not possible. More recently, the diffusion of an HCl trihydrate phase into ice was measured using new laser resonant desorption (LRD) depth-profiling techniques.[48] Based on HCl diffusion measurements from 168 to 195 K, an Arrhenius analysis yielded a diffusion activation barrier of $E_d = 15.3$ kcal mol^{-1} and a diffusion preexponential of $D_0 = 1.5 \times 10^7$ cm^2 s^{-1}.[49] This diffusion activation barrier would predict that the diffusion of HCl hydrates into ice at 140 K is $\sim 3 \times 10^9$ times faster than diffusion at 100 K. The large difference in HCl diffusion rates may easily be able to maintain different steady-state HCl surface coverages. Similar results are expected for HBr.

B. Formation of an HBr Hydrate Phase. The interaction of HBr with ice has been studied by previous molecular beam,[41] flow reactor[17,20] and Knudsen cell[21,23] experiments. The initial HBr sticking coefficient on a pure ice surface is near unity.[41] The HBr uptake coefficient then decreases as HBr builds up on the ice surface and the near surface region of ice. The infrared studies of HBr absorption into ice are consistent with HBr dissociating to form H_3O^+ and Br^-.[23,50] Theoretical calculations are also consistent with facile HBr dissociation in ice.[51] The stable form of HBr in ice is dependent on the ice temperature and the HBr pressure. A phase diagram for HBr−ice has been recently constructed using experimental and theoretical data.[19]

Several questions remain to be answered for HBr absorption into ice. In flow tube experiments, the stoichiometry of stable hydrates has been proposed from H_2O and HBr pressures during the desorption of assumed H_2O/HBr hydrates following HBr uptake on ice.[19] Unfortunately, the desorption mechanism and the validity of the assumption of steady-state equilibrium during desorption in these flow tube experiments should be clarified by additional studies. In addition, the thickness of the H_2O/HBr hydrate on ice is still uncertain. Several previous studies suggest that the H_2O/HBr hydrate is limited to only the top 5−10 monolayers of the ice surface.[19,23] Other studies are consistent with unlimited HBr uptake[17] or the complete conversion of the initial ice film. The exact behavior is probably dependent on

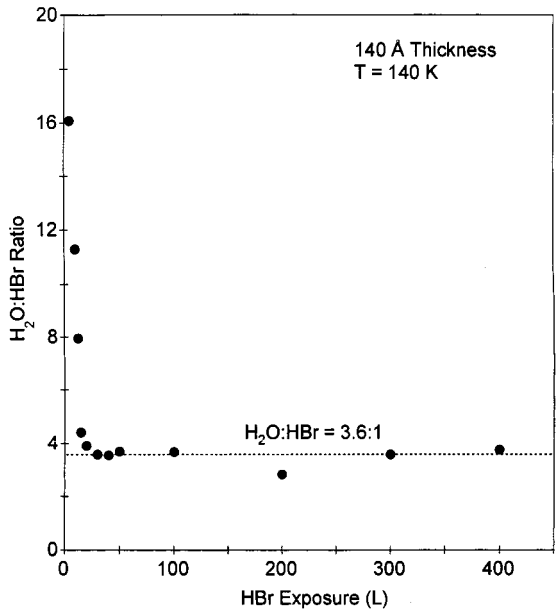

Figure 9. Ratio between the calibrated H_2O and HBr temperature-programmed desorption integrated peak areas versus HBr exposure at 140 K on a 140 Å thick ice film.

the ice film temperature, HBr pressure, HBr exposure time and the thermal history of the ice film.

The TPD results in Figure 3a and the FTIR results summarized in Figure 5 are consistent with the complete conversion of ice films with thicknesses up to at least 400 Å into H_2O/HBr hydrates after HBr exposure at 140 K. The TPD results in Figure 3a indicate that the HBr uptake saturates after large HBr exposures at 140 K. The FTIR results in Figure 5 show that the integrated absorbance of the H_3O^+ band at 1747 cm^{-1} is proportional to the thickness of the initial ice film. This behavior would result from the complete conversion of the ice film into an H_2O/HBr hydrate.

The TPD results in Figure 9 argue for the formation of an H_2O/HBr hydrate with a stoichiometry of ~3.6:1. Experiments using LITD techniques to determine the H_2O:HBr stoichiometry yielded similar results after saturation HBr exposures on ice films at 140 K. A stoichiometry of ~3.6:1 may reflect the presence of a mixture of 3:1 and 4:1 H_2O/HBr crystalline hydrates. Alternatively, the H_2O/HBr hydrate may be amorphous at 140 K. Earlier FTIR studies observed the crystallization of H_2O/HBr hydrates at temperatures from 140 to 160 K.[22,23]

Although the structure of the H_2O/HBr hydrate is not certain, the stoichiometry of ~3.6:1 can be compared with the predicted stoichiometry from an extrapolation of the recent phase diagram for HBr−ice.[19] The phase diagram determines the phase at temperatures from 180 to 250 K.[19] An extrapolation of this phase diagram to 140 K would predict a stoichiometry between 3 and 4:1 at an HBr pressure of $\sim 6 \times 10^{-8}$ Torr. Consequently, the observed ~3.6:1 stoichiometry is consistent with the recent phase diagram.

Crystalline hydrates with composition $n$$H_2O$:HBr where $n = 1-4$ have been identified by X-ray crystallography.[52] These crystalline hydrates were prepared by mixing the appropriate molar ratios of H_2O and HBr. Besides X-ray analysis, the existence of various H_2O/HBr hydrates has been observed by early infrared spectroscopy studies.[53] Equal molar amounts of H_2O and HBr were initially deposited on cooled substrates. Upon heating, different spectra evolved that were assigned as H_2O/HBr monohydrate, dihydrate, trihydrate and tetrahydrate.[53] These assignments assumed that the H_2O/HBr monohydrate was formed on condensation of the equimolar gas mixtures. The results of this earlier infrared study have been clarified by more recent infrared studies.[22,37]

The FTIR and TPD results of this study are consistent with the complete conversion of ice films with thicknesses up to at least 400 Å at 140 K. The stoichiometry of the resultant H_2O/HBr hydrate is consistent with a mixture of 3:1 and 4:1 crystalline H_2O/HBr hydrates or an amorphous H_2O/HBr hydrate. Only a thin layer of H_2O/HBr hydrate is formed in the flow tube experiments on much thicker ice films.[19] This behavior may be explained by changes in HBr solubility at higher ice film temperatures dictated by the HBr−ice phase diagram.[19] The limited absorption of HBr of ~20 ML observed by other recent HBr uptake studies at 110 K[23] may be dictated by low HBr diffusion rates at 110 K.

C. H_2O Desorption Kinetics from Ice Films Exposed to HBr. Figure 3 shows that pure H_2O films with a thickness of 140 Å and the ice films with a thickness of 140 Å exposed to >80 L HBr display single H_2O TPD peaks at ~168 K and ~178 K, respectively. The H_2O TPD spectra of ice films subjected to intermediate HBr exposures combine characteristics of both pure ice and ice films saturated with HBr. The initial splitting of the H_2O TPD peak and shift to higher temperatures begins at low HBr coverages after HBr exposures of ~4 L. The low-temperature H_2O peak is negligible after the higher HBr exposures of 17 and 83 L.

The FTIR results for the H_3O^+ band at 1747 cm^{-1} are in very close correspondence with the splitting of the H_2O TPD peaks and the shift of the H_2O TPD peak to higher temperatures. The H_3O^+ absorption band grows versus HBr exposure as the H_2O TPD peak is split into low and high temperature features. The H_3O^+ absorption intensity reaches its maximum level after HBr exposures >80 L when only the high-temperature peak is observed in the H_2O TPD spectrum.

The H_2O desorption rate from pure H_2O multilayers should follow zero-order kinetics, $-d\Theta/dt = \nu_0 \exp(-E_d/RT)$, where E_d is the desorption activation energy and ν_0 is the zero-order desorption preexponential.[27,54−56] The desorption kinetic parameters, E_d and ν_0, can be derived from the H_2O TPD data shown in Figure 6. The H_2O TPD signals were first calibrated to determine the absolute desorption rate, $d\Theta/dt$. The Arrhenius plot of $\ln(d\Theta/dt)$ versus inverse temperature ($1000/T$) is displayed in Figure 10 for both a 130 Å thick pure ice film and a 130 Å thick ice film after a 756 L HBr exposure.

For H_2O desorption from pure ice films, the desorption activation energy is $E_d = 13.4 \pm 0.3$ kcal mol^{-1} and the zero-order desorption preexponential is $\nu_0 = 1.9 \times 10^{32} \pm 0.025 \times 10^{32}$ cm^{-2} s^{-1}. These results are in good agreement with previous H_2O desorption measurements[27,54−56]. For the ice films exposed to 42, 84, and 756 L HBr, the desorption activation energy is $E_d = 10.6 \pm 0.2$ kcal mol^{-1} and the zero-order preexponential is $\nu_0 = 6.31 \times 10^{27} \pm 0.04 \times 10^{27}$ cm^{-2} s^{-1}. These kinetic parameters can be utilized to fit the leading edge of the H_2O TPD spectrum from the pure ice film and the ice films subjected to HBr exposures shown in Figure 6. The predicted desorption rates from the kinetic parameters are in excellent agreement with the experimental results.

Figure 7 reveals that H_2O desorption following a fixed HBr exposure of 32 L at 140 K is dependent on the ice film thickness. For small thicknesses of 105 Å, only the high-temperature H_2O peak is observed that is consistent with the saturated H_2O/HBr hydrate. For larger ice film thicknesses of 190 and 300 Å, both the high and low-temperature peaks are visible. For even thicker ice films of 425 and 670 Å, the H_2O desorbs primarily from

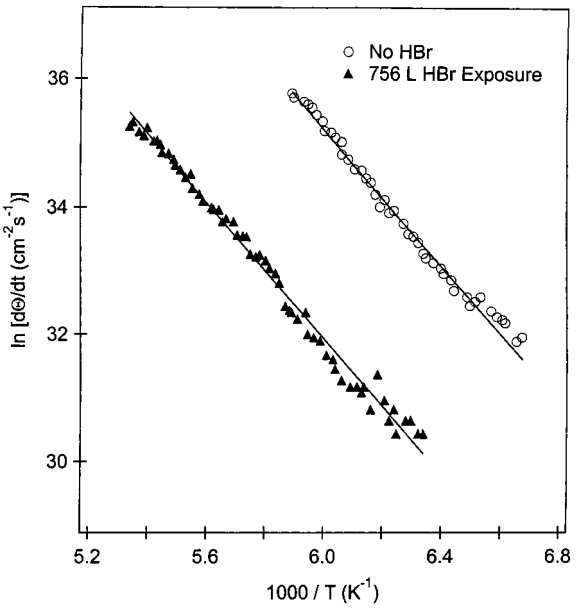

Figure 10. Arrhenius plot of ln(dΘ/d*t*) versus 1000/*T* obtained from the temperature-programmed desorption of H_2O from a pure 130 Å thick ice film and 130 Å thick ice film after an HBr exposure of 756 L at 140 K. The open circles and solid triangles show the experimental data from Figure 6. The solid lines display the linear least-squares fits to the data that yield the desorption kinetic parameters.

the low-temperature H_2O peak. These H_2O desorption results can be understood in terms of an inadequate supply of HBr to convert the ice films into a saturated H_2O/HBr hydrate during the 32 L HBr exposure at 140 K.

The ice film with a thickness of 105 Å can be nearly completely converted to the H_2O/HBr hydrate during the 32 L HBr exposure. An ice film with a thickness of 105 Å and a density of 0.93 g/cm^3 has an H_2O coverage of 3.3×10^{16} cm^{-2}. Assuming a unity sticking coefficient, the 32 L HBr exposure corresponds to a resultant HBr coverage of 7.2×10^{15} cm^{-2}. For an H_2O/HBr hydrate with a stoichiometry of ~3.6:1, the 105 Å ice film requires 9.1×10^{15} HBr molecules to reach saturation. Consequently, the 105 Å thick ice film can be nearly completely converted to the saturated H_2O/HBr hydrate. The thicker films are only partially converted to the saturated H_2O/HBr hydrate because the HBr exposure does not provide enough HBr molecules to reach a ~3.6:1 stoichiometry.

Figure 8 explores the effect of ice film temperature on H_2O desorption following a 32 L HBr exposure on a 130 Å thick ice film. Only a high-temperature H_2O desorption peak is observed after the 32 L HBr exposure at 140 K in agreement with Figure 7. After HBr exposure at progressively lower ice film temperatures, the low-temperature H_2O desorption peak grows and nearly dominates the H_2O desorption when the ice film temperature reaches 90 K. This behavior is explained by slower HBr diffusion into the ice film at lower temperature. Slower HBr diffusion limits HBr absorption into the ice bulk and maintains high HBr surface coverages that reduce the HBr uptake coefficient. Corresponding HBr TPD signals are consistent with less HBr absorption at the lower temperatures following the 32 L HBr exposure.

V. Conclusions

Laser-induced thermal desorption (LITD), temperature-programmed desorption (TPD) and Fourier transform infrared (FTIR) spectroscopy techniques were used to examine the uptake of HBr on thin ice films at low temperatures. LITD measurements obtained an uptake coefficient for HBr on ice of $\gamma = 0.61 \pm 0.06$ at 140 K and $\gamma = 0.24 \pm 0.05$ at 100 K. TPD measurements determined that thin ice films exposed to HBr at 140 K became saturated after large HBr exposures. The TPD results determined that the saturated H_2O/HBr hydrate had a stoichiometry of ~3.6:1. Corresponding FTIR measurements monitored the development of the H_3O^+ bending vibration and observed the saturation of the integrated absorbance for the H_3O^+ bending vibration after large HBr exposures. H_2O desorption from ice was significantly perturbed by the uptake of HBr on ice and H_2O desorbed at higher temperatures in the presence of HBr. After saturation HBr exposures, the zero-order kinetics for H_2O desorption from the H_2O/HBr hydrate were $E_d = 10.6$ kcal mol^{-1} and $\nu_0 = 6.3 \times 10^{27}$ cm^{-2} s^{-1}.

Acknowledgment. This research was funded by the National Science Foundation by Grants CHE-9905812 (S.M.G.), CHE-9614134 and CHE-9988434 (V.H.G.), and ATM-9711969 (M.A.T.). Additional support was provided by NASA-SASS SA98-0005 (M.A.T.).

References and Notes

(1) Barrie, L. A.; Bottenheim, J. W.; Schnell, R. C.; Crutzen, P. J.; Rasmussen, R. A. *Nature* **1988**, *334*, 138.
(2) Bottenheim, J. W.; Barrie, L. A.; Atlas, E.; Heidt, L. E.; Niki, H.; Rasmussen, R. A.; Shepson, P. B. *J. Geophys. Res.−Atmos.* **1990**, *95*, 18555.
(3) Leaith, W. R.; Barrie, L. A.; J. Bottenheim, W.; Li, S. M.; Shepson, P. B.; Muthuramu, K.; Yokouchi, V. *J. Geophys. Res.−Atmos.***1994**, *99*, 25499.
(4) Hausmann, M.; Platt, U. *J. Geophys. Res.−Atmos.* **1994**, *99*, 25399.
(5) McElroy, C. T.; McLinden, C. A.; McConnell, J. C. *Nature* **1999**, *397*, 338.
(6) Impey, G. A.; Shepson, P. B.; Hastie, D. R.; Barrie, L. A.; Anlauf, K. G. *J. Geophys. Res.* **1997**, *102*, 16005.
(7) McConnell, J. C.; Henderson, G. S.; Barrie, L.; Bottenheim, J.; Niki, H.; Langford, C. H.; Templeton, E. M. J. *Nature* **1992**, *355*, 150.
(8) Fan, S. M.; Jacob, D. J. *Nature* **1992**, *359*, 522.
(9) Andreae, M. O.; Crutzen, P. J. *Science* **1997**, *276*, 1052.
(10) Oum, K. W.; Lakin, M. J.; Finlayson-Pitts, B. J. *Geophys. Res. Lett.* **1998**, *25*, 3923.
(11) Tang, T.; McConnell, J. C. *Geophys. Res. Lett.* **1996**, *23*, 2633.
(12) *Chemical Kinetics and Photochemical Data for Use in Stratospheric Modeling*; DeMore, W. B., Sander, S. P., Golden, D. M., Hampson, R. F., Kurylo, M. J., Howard, C. J., Ravishankara, A. R., Kolb, C. E., Molina, M. J., Eds.; NASA/Jet Propulsion Laboratory: Pasadena, CA, 1997.
(13) Sumner, A. L.; Shepson, P. B. *Nature* **1999**, *398*, 230.
(14) Abbatt, J. P. D. *Geophys. Res. Lett.* **1994**, *21*, 665.
(15) Abbatt, J. P. D.; Nowak, J. B. *J. Phys. Chem. A* **1997**, *101*, 2131.
(16) Chu, L.; Chu, L. T. *J. Phys. Chem. A* **1999**, *103*, 691.
(17) Hanson, D. R.; Ravishankara, A. R. *J. Phys. Chem.* **1992**, *96*, 9441.
(18) Chu, L. T.; Heron, J. W. *Geophys. Res. Lett.* **1995**, *22*, 3211.
(19) Chu, L.; Chu, L. T. *J. Phys. Chem. A* **1999**, *103*, 384.
(20) Percival, C. J.; Mossinger, J. C.; Cox, R. A. *Phys. Chem. Chem. Phys.* **1999**, *1*, 4565.
(21) Fluckiger, B.; Thielmann, A.; Butzwiller, L.; Rossi, M. J. *Ber. Bunsen-Ges. Phys. Chem.* **1998**, *102*, 915.
(22) Carlo, S. R.; Grassian, V. H. *J. Phys. Chem. B* **2000**, *104*, 86.
(23) Barone, S. B.; Zondlo, M. A.; Tolbert, M. A. *J. Phys. Chem. A* **1999**, *103*, 9717.
(24) Foster, K. L.; Tolbert, M. A.; George, S. M. *J. Phys. Chem. B* **1997**, *101*, 4979.
(25) Berland, B. S.; Tolbert, M. A.; George, S. M. *J. Phys. Chem. A* **1997**, *101*, 9954.
(26) Tro, N. J.; Haynes, D. R.; Nishimura, A. M.; George, S. M. *J. Chem. Phys.* **1989**, *91*, 5778.
(27) Haynes, D. R.; Tro, N. J.; George, S. M. *J. Phys. Chem.* **1992**, *96*, 8502.
(28) Myli, K. B.; Grassian, V. H. *J. Phys. Chem.* **1995**, *99*, 1498.
(29) Arthur, D. A.; Meixner, D. L.; Boudart, M.; George, S. M. *J. Chem. Phys.* **1991**, *95*, 8521.
(30) George, S. M.; DeSantolo, A. M.; Hall, R. B. *Surf. Sci.* **1985**, *159*, L425.
(31) Berland, B. S.; Haynes, D. R.; Foster, K. L.; Tolbert, M. A.; George, S. M.; Toon, O. B. *J. Phys. Chem.* **1994**, *98*, 4358.
(32) Berland, B. S.; Brown, D. E.; Tolbert, M. A.; George, S. M. *Geophys. Res. Lett.* **1995**, *22*, 3493.
(33) Born, M.; Wolf, E. *Principles of Optics*; Pergamon Press: Oxford, U.K., 1975.

(34) Eisenberg, D.; Kauzmann, W. *The Structure and Properties of Water*; Oxford University Press: New York, 1969.
(35) Timmermans, J. *The Physico-Chemical Constants of Binary Systems in Concentrated Solutions, Volume 4, Systems with Inorganic + Organic or Inorganic Compounds*; Interscience Publishers: New York, 1960.
(36) *CRC Handbook of Chemistry and Physics*; Weast, R. C., Ed.; CRC Press: Boca Raton, FL, 1983; Vol. 64.
(37) Delzeit, L.; Rowland, B.; Devlin, J. P. *J. Phys. Chem.* **1993**, *97*, 10312.
(38) Thiel, P. A.; Madey, T. E. *Surf. Sci. Rep.* **1987**, *7*, 211.
(39) Hagen, W.; Tielens, A. G. G. M.; Greenberg, J. M. *Chem. Phys.* **1981**, *56*, 367.
(40) Horn, A. B.; Banham, S. F.; McCoustra, M. R. S. *J. Chem. Soc., Faraday Trans.* **1995**, *91*, 4005.
(41) Rieley, H.; Allen, H. D.; Haq, S. *J. Chem. Soc., Faraday Trans.* **1995**, *91*, 2349.
(42) Isakson, M. J.; Sitz, G. O. *J. Phys. Chem. A* **1999**, *103*, 2044.
(43) Andersson, P. U.; Nagard, M. B.; Pettersson, J. B. C. *J. Phys. Chem. B* **2000**, *104*, 1596.
(44) Kroes, G. J.; Clary, D. C. *J. Phys. Chem.* **1992**, *96*, 7079.
(45) Wang, L.; Clary, D. C. *J. Chem. Phys.* **1996**, *104*, 5663.
(46) Pruppacher, H. R.; Klett, J. D. *Microphysics of Clouds and Precipitation*; D. Reidel Publishing: Dordrecht, Holland, 1978.
(47) Thibert, E.; Domine, F. *J. Phys. Chem. B* **1997**, *101*, 3554.
(48) Livingston, F. E.; Smith, J. A.; George, S. M. *Anal. Chem.* **2000**, *72*, 5590.
(49) Livingston, F. E.; George, S. M. *J. Phys. Chem.*, submitted.
(50) Peil, S.; Seisel, S.; Schrems, O. *J. Mol. Struct.* **1995**, *348*, 449.
(51) Gertner, B. J.; Peslherbe, G. H.; Hynes, J. T. *Isr. J. Chem.* **1999**, *39*, 273.
(52) Lundgren, J. O. *Acta Crystallogr.* **1970**, *B26*, 1893.
(53) Gilbert, A. S.; Sheppard, N. *J. Chem. Soc., Faraday Trans.* **1973**, *69*, 1628.
(54) Livingston, F. E.; Smith, J. A.; George, S. M. *Surf. Sci.* **1999**, *423*, 145.
(55) Brown, D. E.; George, S. M.; Huang, C.; Wong, E. K. L.; Rider, K. B.; Smith, R. S.; Kay, B. D. *J. Phys. Chem.* **1996**, *100*, 4988.
(56) Brown, D. E.; George, S. M. *J. Phys. Chem.* **1996**, *100*, 15460.